Introduction to the Phase Contrast Radiography, X-Ray Microtomography and Holotomography

Franco Rustichelli

Università Politecnica delle Marche
Istituto Nazionale Biostrutture e Biosistemi (INBB)

RADIOGRAPHY (X-ray absorption)

Suppose that a monochromatic radiation X hits on a slab of homogeneous material whose thickness is x (a).

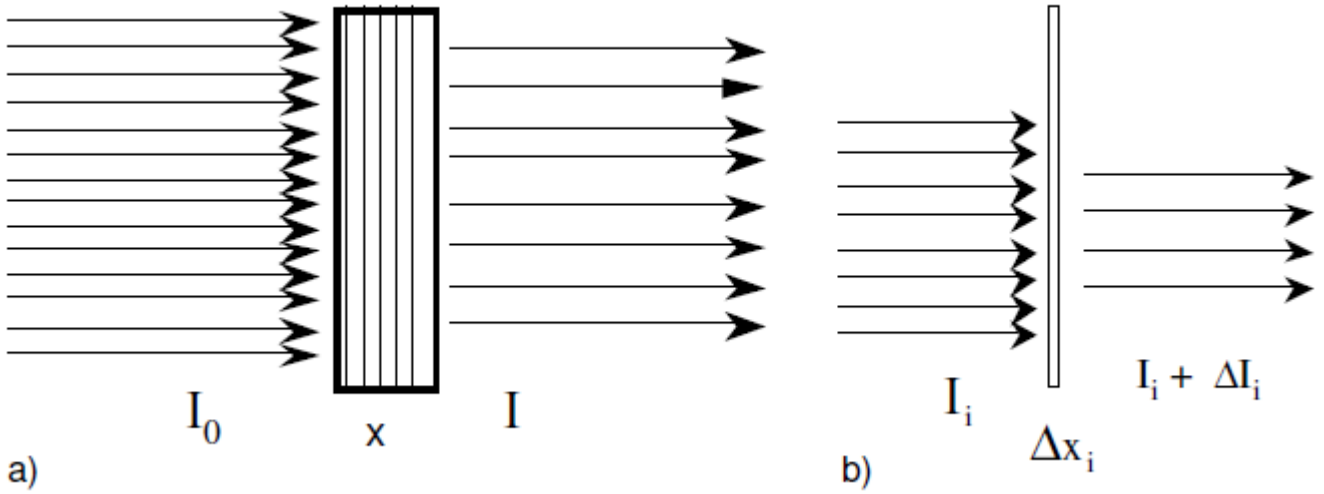

If the incident intensity of the radiation is I_0 from the plate a beam with attenuated intensity I emerges. Imagine divide the plate into many very thin slices each of thickness Dx. Consider in Figure 4b the ith slice. If the incident intensity
of the X radiation is **I**i, it will suffer the attenuation ΔII (<0). Experimentally it is possible to see that for a very thin slab the attenuation is:

$$\Delta I_i = - \mu I_i \Delta x_i \qquad \frac{\Delta I_i}{I_i} = - \mu \Delta x_i$$

Δii is proportional to the thickness Δx_i, to the initial intensity $\mathbf{I}_i$ and coefficient μ that depends from the incident radiation frequency and the material.

We suppose now the attenuations for Δ II / $\mathbf{I}_i$ on the all other slices, to take into account the thickness x of the plate:

$$\Sigma_i \frac{\Delta I_i}{I_i} = - \mu \Sigma_i \Delta x_i$$

Passing at the limit we obtain (ΔI and Δx tend at the same time to limit)

$$\lim_{\Delta I_i \to 0} \sum_{1}^{n} \frac{\Delta I_i}{I_i} = -\mu \lim_{\Delta x_i \to 0} \sum_{1}^{n} \Delta x_i$$

$$\ln \frac{I_x}{I_0} = -\mu x \quad \Rightarrow \quad \frac{I_x}{I_0} = e^{-\mu x} \quad \Rightarrow \quad I_x = I_0 \, e^{-\mu x}$$

This is the exponential law of radiation X absorption in the materials

…and the graphic representation is:

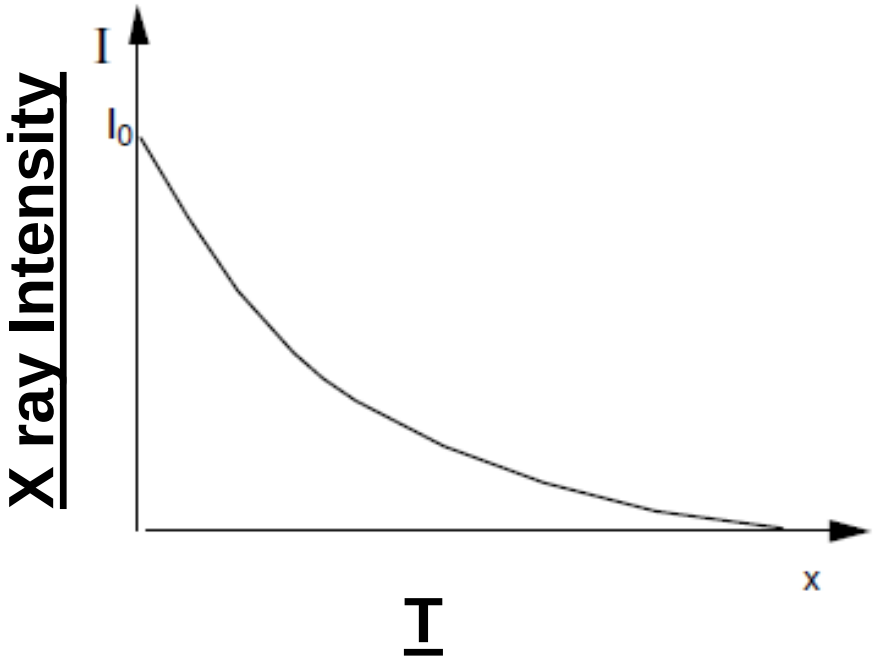

The absorption coefficent μ depends from the wave lenght of the incident radiation and form the kind of used material. In the X radiography for the medical use the organs have a different absorption coefficients. It results a contrast that it can put in evidence the several parts, being different the X- ray “transparency”.

When the natural contrast is weak it is possible to increase it ingesting or injecting some “dull” substances

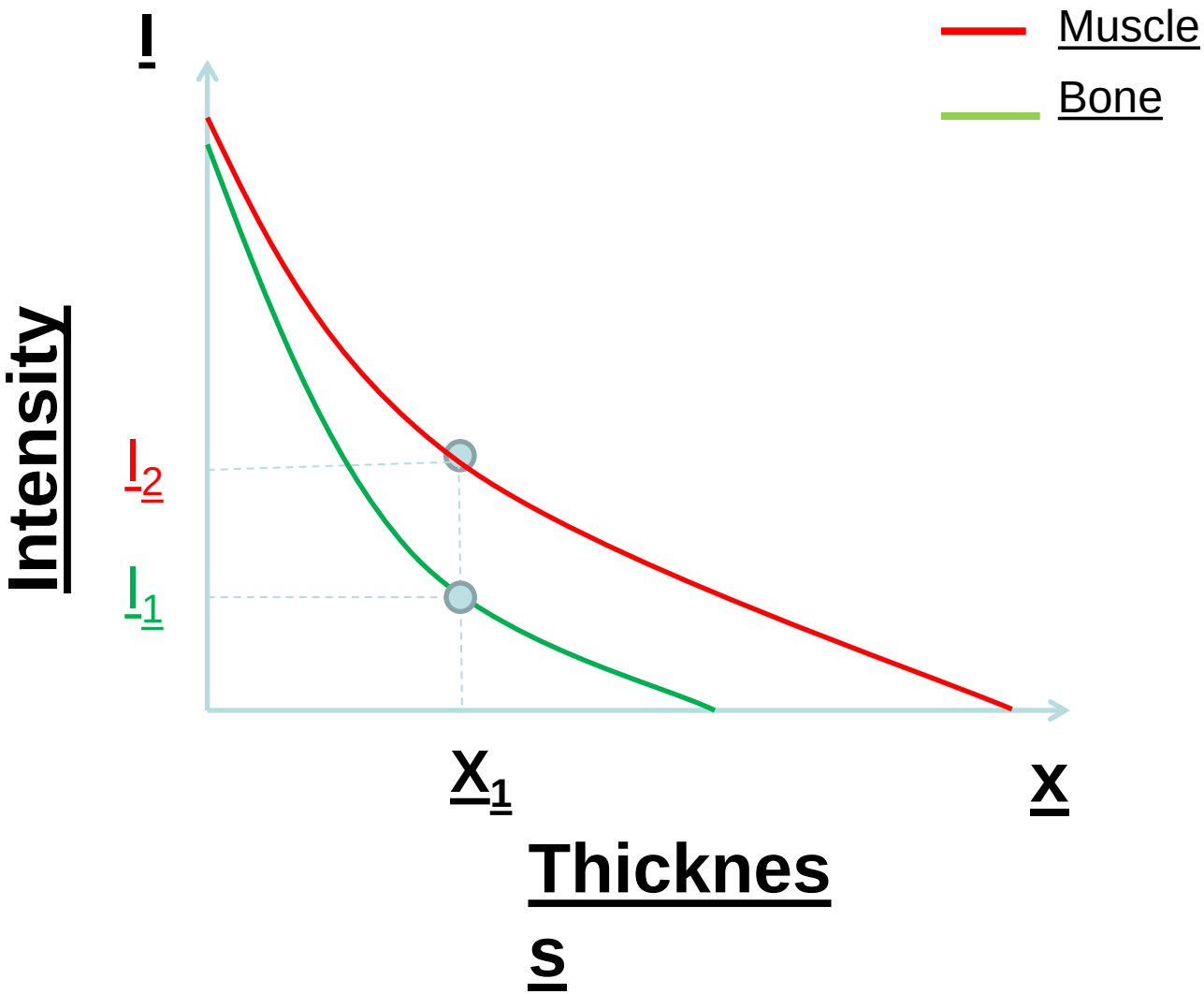

In conventional radiography, when X-rays pass through an object the resulting emerging beam gives information about the absorption occurred within the sample.

Phase-contrast imaging consists in the recording of phase variations of the radiation passing through the sample.
Phase gradients are detected using diffraction from perfect crystals.

Aim of the Phase-contrast imaging experiments is the recording of phase contrast images of items and their comparison with the relative absorption-contrast based radiographs.

Phase-Contrast Imaging

Sample

X-Rays

$$E(\vec{r}) = A_0 e^{-i\vec{k}\vec{r}}$$

absorbtion

$$A(z) = A_0 e^{-\beta z/2}$$

β **= absorbtion index**

Phase Change

$$A(z) = A_0 e^{-i\delta z}$$

δ **= Refraction index**

n=1-δ+iβ

Complex refractive index

5 keV < E < 60 keV

2.5 Å < λ < 0.1 Å

INTERFERENCE

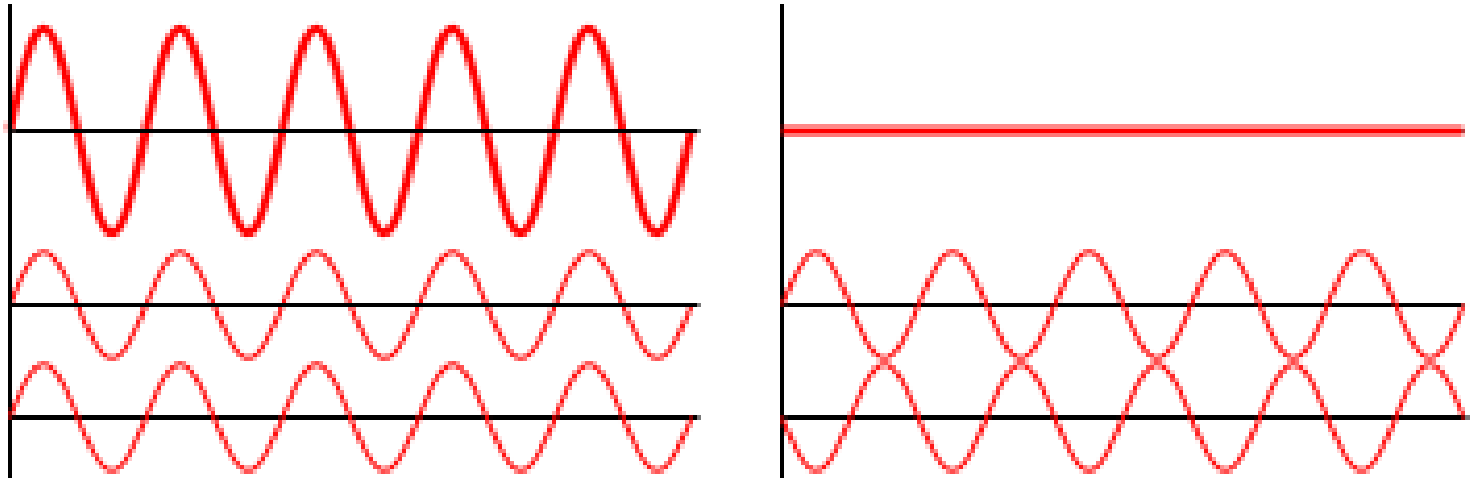

The interference of two waves. When in phase, the two lower waves create constructive interference (left), resulting in a wave of greater amplitude. When 180° out of phase, they create destructive interference (right).

Phase-contrast imaging experimental set-up at GILDA – Esrf (Grenoble)

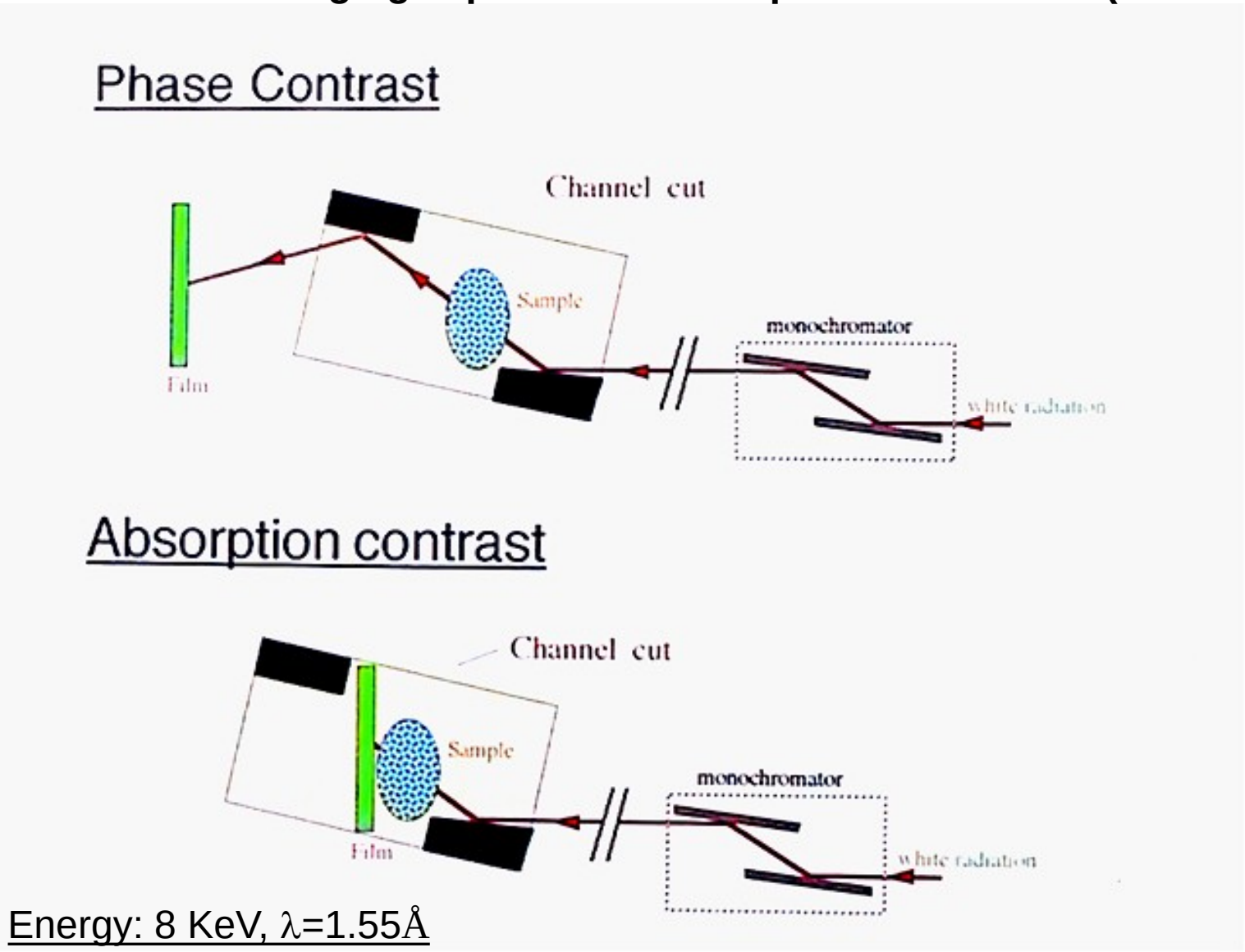

Energy: 8 KeV, λ=1.55Å

Phase-Shift detection

1)diffraction

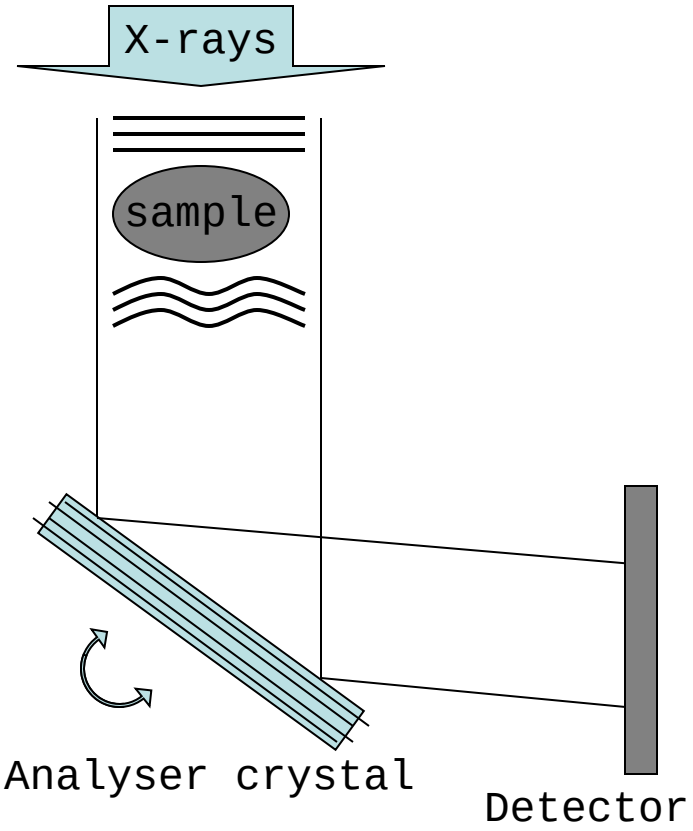

Experiments at GILDA-ESRF

2)free propagation

(high spatial coherence needed)

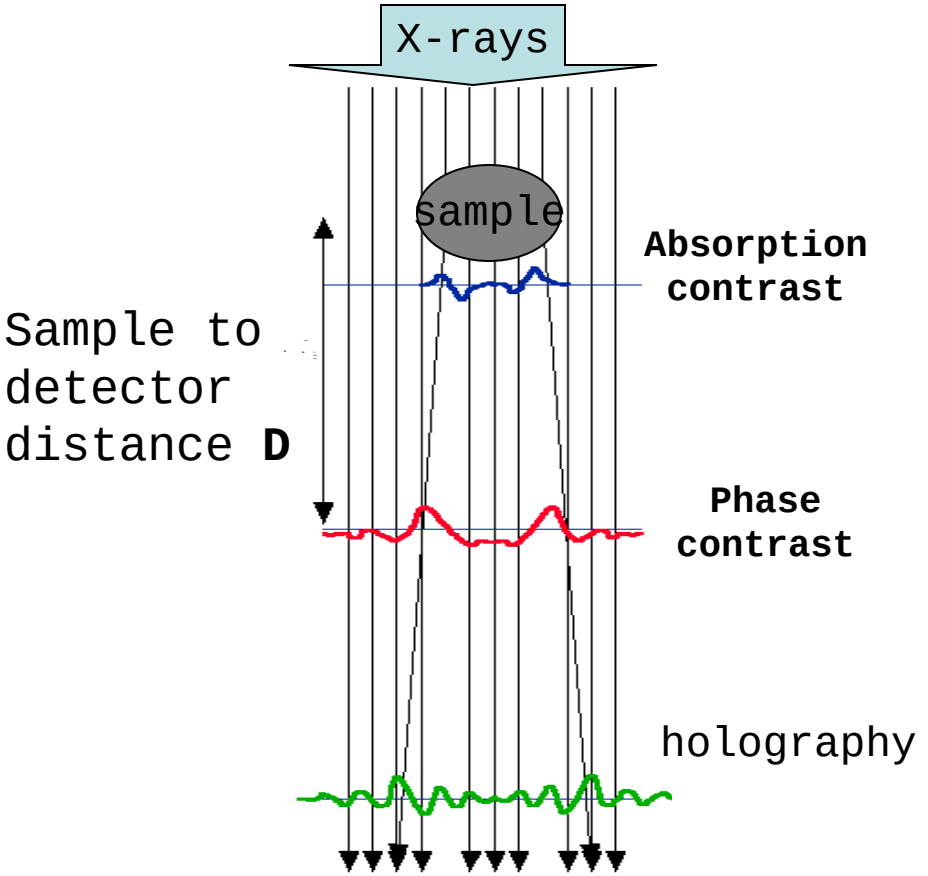

Experiments at beamline ID19-ESRF

Phys. Med. Biol. **46** (2001) 967–974 www.iop.org/Journals/pb PII: S0031-9155(01)17424-5

Curved optics for x-ray phase contrast imaging by synchrotron radiation

S Colonna[1], F D'Acapito[2], S Mobilio[3], S Onori[4], L Pugliani[4], S Romanzetti[5] and F Rustichelli[5]

[1] CNR-GILDA crg ESRF B.P. 220, F-38043 Grenoble Cedex, France
[2] INFM OGG-GILDA crg ESRF B.P. 220, F-38043 Grenoble Cedex, France
[3] Dip. di Fisica, Università di Roma Tre, Via della Vasca Navale 84, I-00146, Roma, Italy and Laboratori Nazionali di Frascati INFN via E Fermi 40, I-00044 Frascati, Italy
[4] Istituto Superiore di Sanità and INFN Gruppo Collegato Sanità, Viale Regina Elena 299, I-00161, Roma, Italy
[5] Istituto di Scienze Fisiche–Università di Ancona, Via P Ranieri 65, I-60131, Ancona, Italy and INFN Gruppo Collegato Sanità, Viale Regina Elena 299, I-00161, Roma, Italy

Received 26 September 2000, in final form 12 December 2000

We investigated a huge number of samples, most of all biological tissues.
In particular, we concentrated our experiments at GILDA (ESRF, Grenoble) on a butterfly for its low absorption coefficient (in the wings) and for the very large content of edges (i.e. refractive index variations).
This sample was very interesting, from an experimental point of view, because it allowed us to have a deeper knowledge of the technique and to compare conventional radiographs with the phase-contrast one.

Università Politecnica delle Marche (UNIVPM)

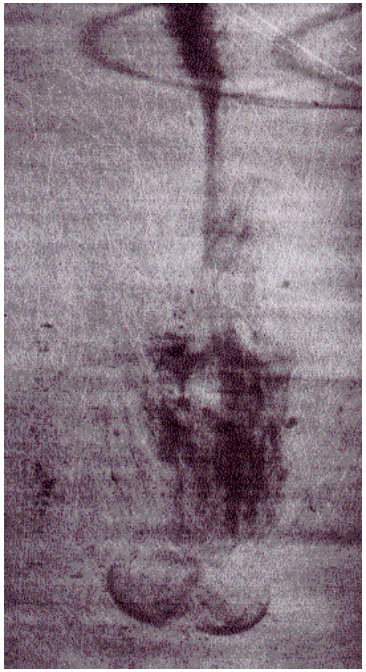

Phase-contrast (left) and absorption-contrast (right) radiographs on a butterfly.

nature
INTERNATIONAL WEEKLY JOURNAL OF SCIENCE
Volume 384 Nor 6607 #28 November 1996 ...00 FFr4... DM17.5 Lire13000 A$12

Phase-contrast radiography

The signature of interstellar H_3^+

Surviving heart failure

A *dwarf* prophet

DNA technology
PRODUCT REVIE

ELSEVIER

Biomaterials 22 (2001) 1515–1520

Biomaterials

www.elsevier.com/locate/biomaterials

Phase-contrast imaging of thin biomaterials

J. Baruchel[a], A. Lodini[b], S. Romanzetti[c,*], F. Rustichelli[c], A. Scrivani[d]

[a]*ESRF, 38043 Grenoble, France*
[b]*Laboratoire Leon Brillouin CEA/Saclay, 91191 Gif-Sur-Yvette Cedex, France*
[c]*Istituto di Scienze Fisiche, Universitá degli Studi di Ancona and INFN, Via P. Ranieri, 65 I-60131 Ancona, Italy*
[d]*FLAMETAL SpA, Via G. Di Vittorio, 51, I-43045 Fornovo di Taro (PR), Italy*

Received 15 December 1999; accepted 8 October 2000

Dependence of sample-to-detector distance D on image formation

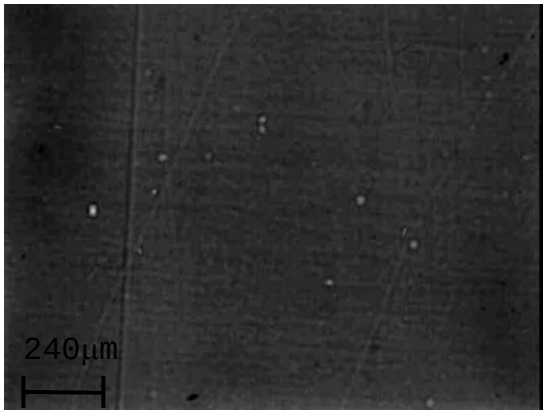

D=1.5 cm

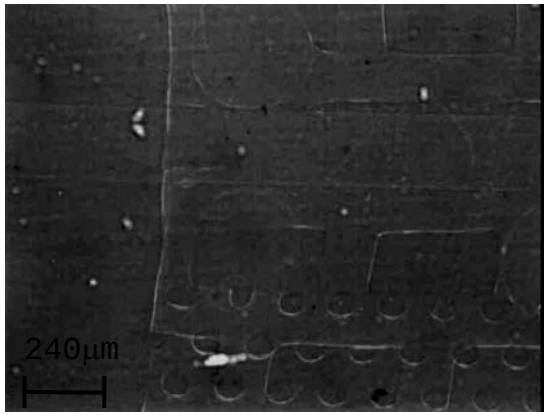

D=15 cm

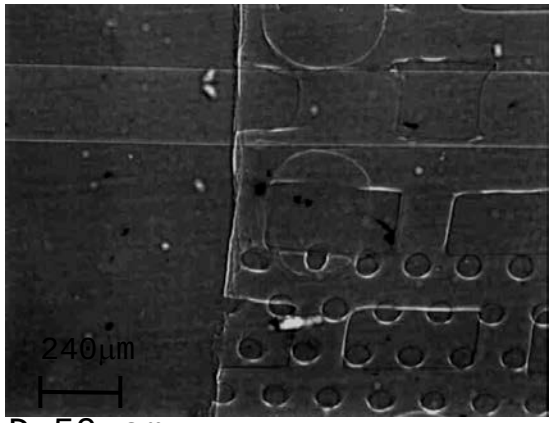

D=50 cm

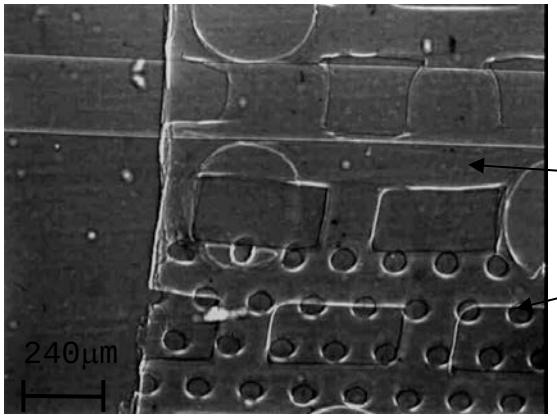

D=100 cm

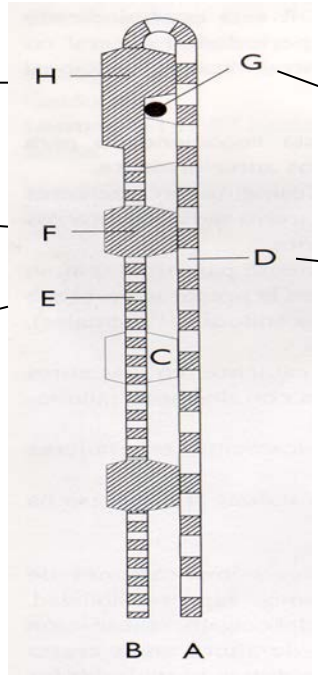

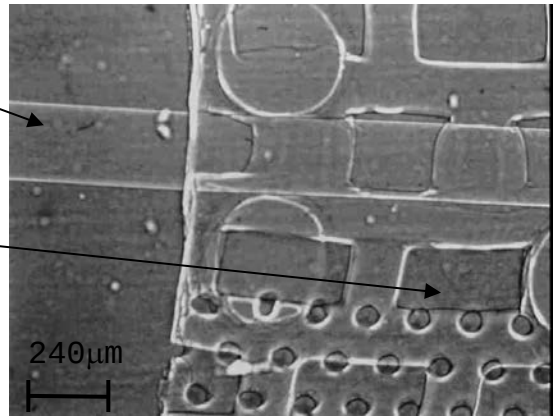

D=150 cm

GUIDOR matrix bioresorbable barrier

Romanzetti S et.al BIOMATERIALS, 22 (12): 1515-1520 JUN 2001

Absorption contrast

Gingival cyst

Phase contrast

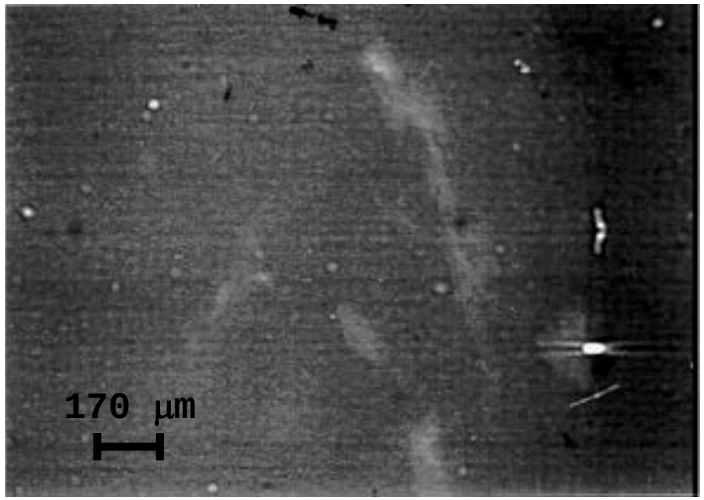

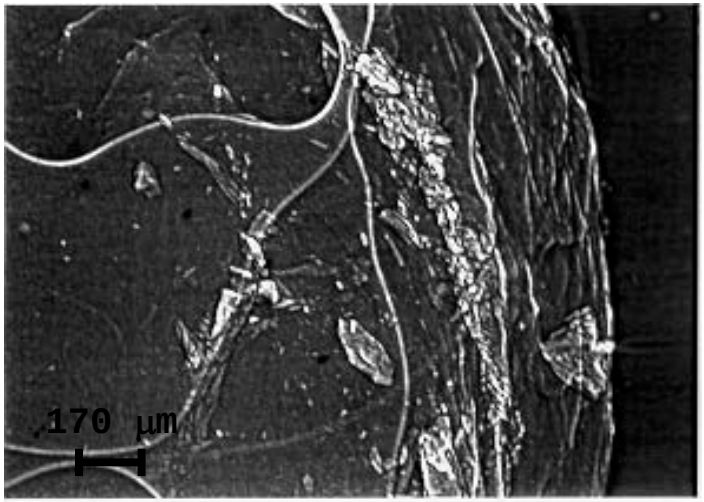

Absorption contrast

Alveolate bone

Phase contrast

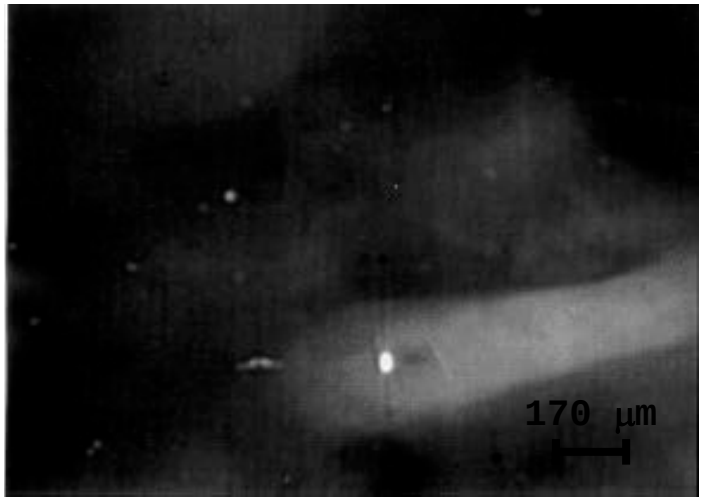

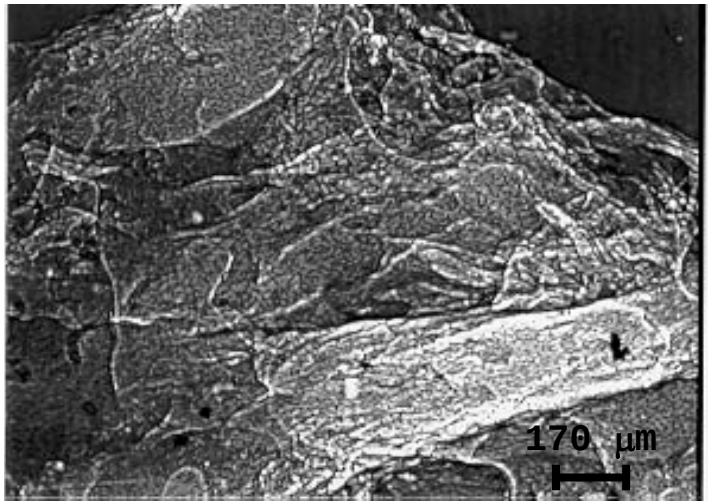

Images recorded at the beamline ID19 – ESRF – Grenoble
E= 25 KeV; λ=0.49 Å

Uterus Slice

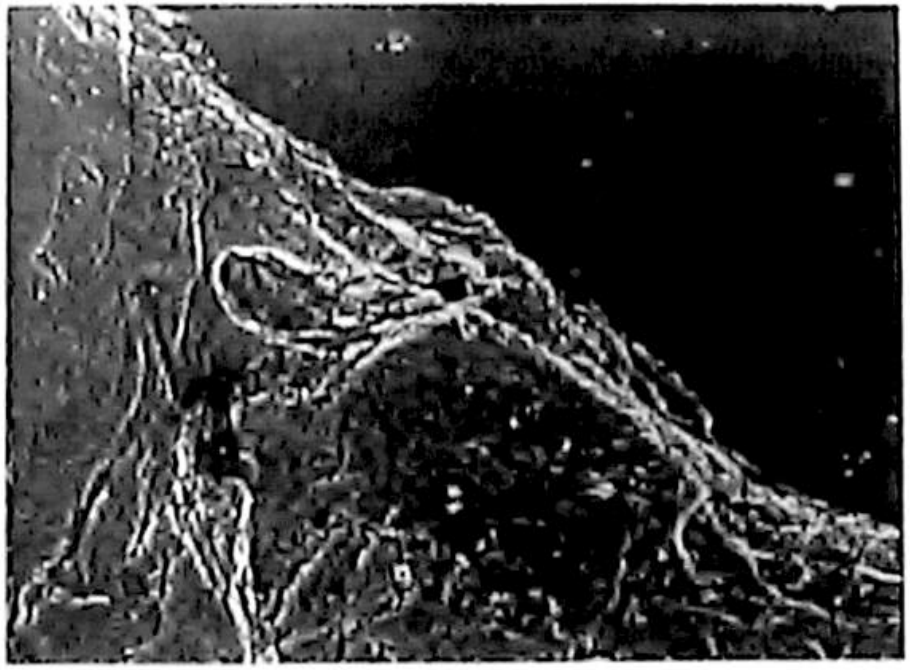

Phase contrast Image

X-ray Computed Microtomography System at ESRF

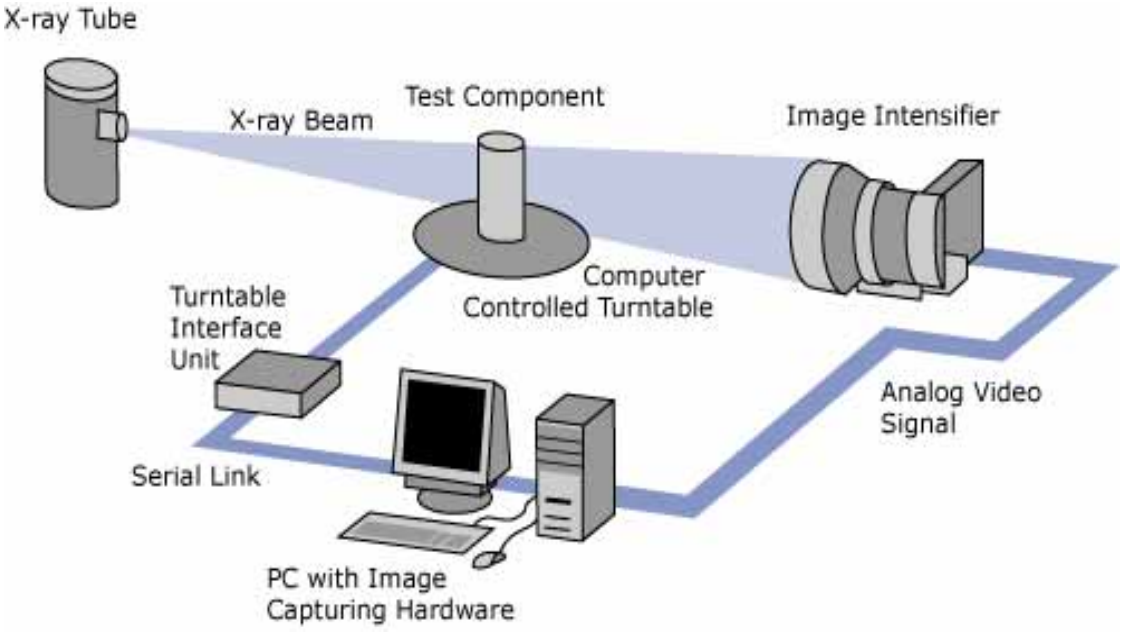

Schematic set up of microCT system installed at ID19 in ESRF

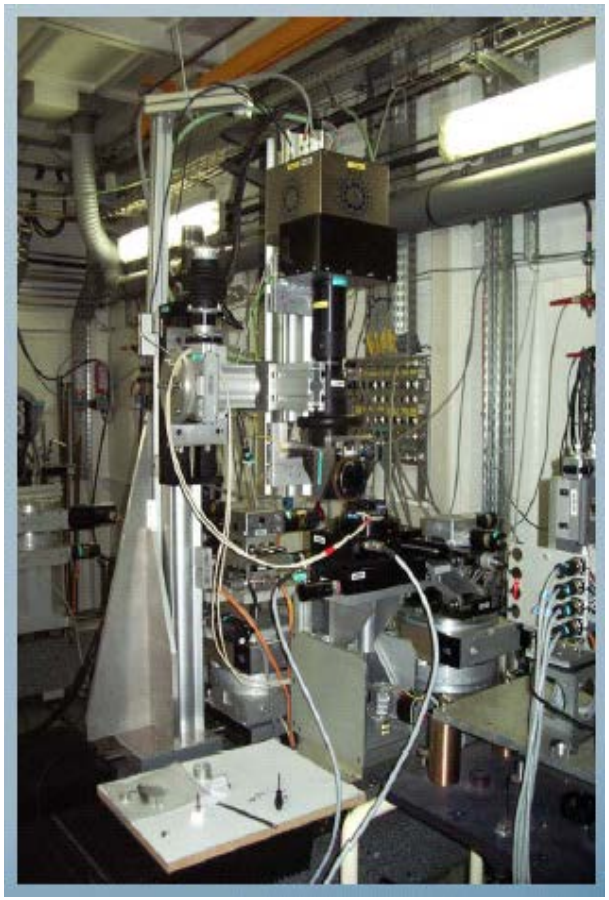

Kinetics of *in vivo* bone deposition by bone marrow stromal cells into non-resorbable and resorbable ceramic scaffold: X-ray computed microtomography

Vladimir S. Komlev, Maddalena Mastrogiacomo, Francoise Peyrin, Ranieri Cancedda, Franco Rustichelli

TISSUE ENGINEERING: Volume 12, Number 12, (2006)

Testing of a New Scaffold for Bone Repair

✓nude mouse model

(screening of osteogenic cells and scaffolds)

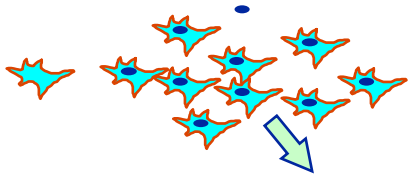

Bone Marrow Stromal Cells from iliac crest of sheep

Subcutaneous implantation in immunodeficient mice

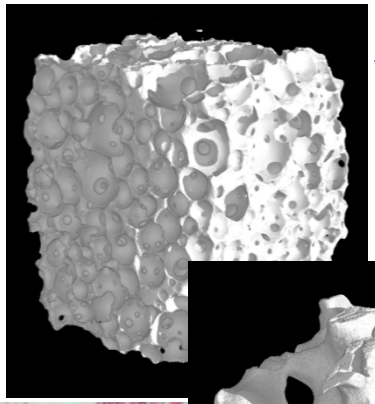

HA Porous Bioceramics

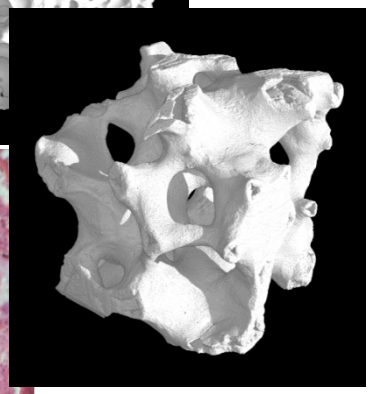

Silicon-stabilized Tricalcium Phosphate Porous Bioceramics

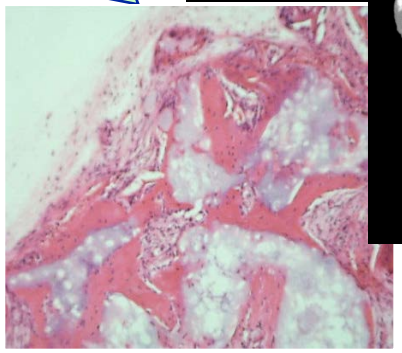

New Bone formation

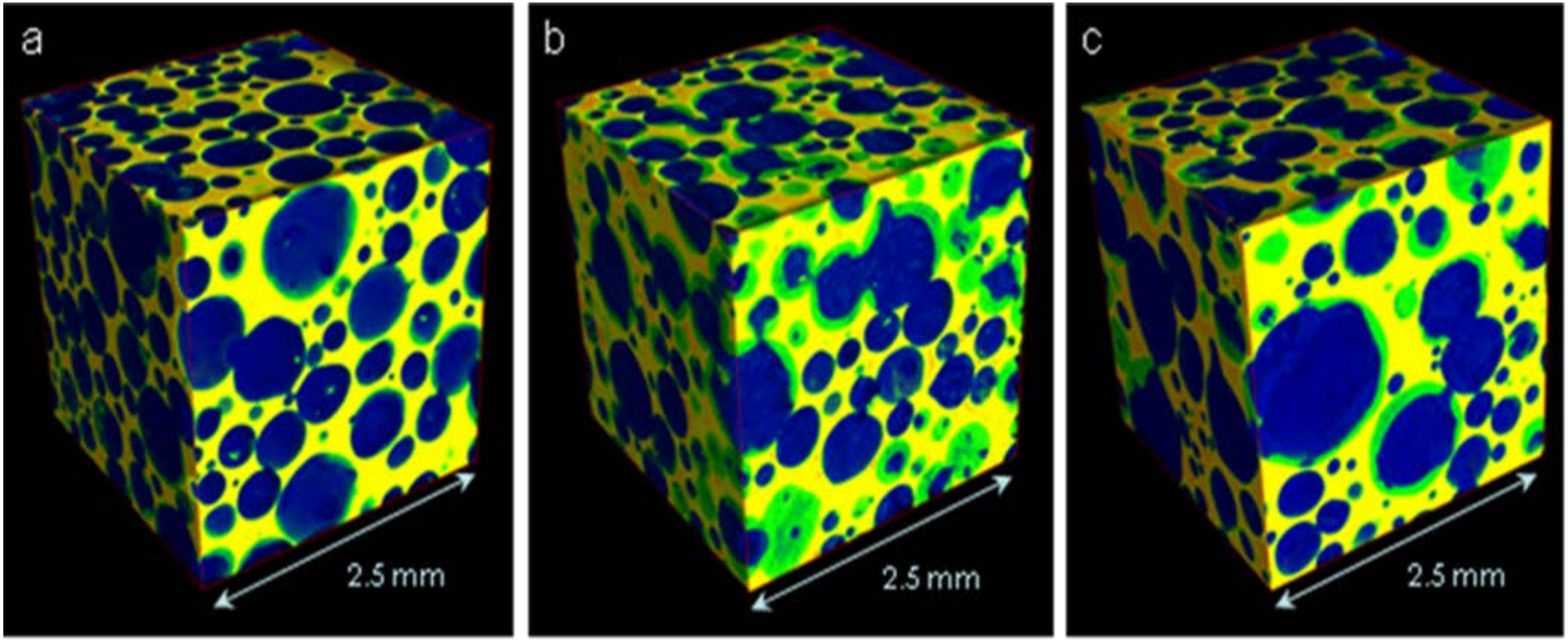

3D display of sub volume of scaffolds after the implant at 8 (a), 16 (b) and 24 (c) weeks. The images show the new bone (green) onto the inner surface of scaffold (yellow). The other phases (e.g. organic phase) is blue.

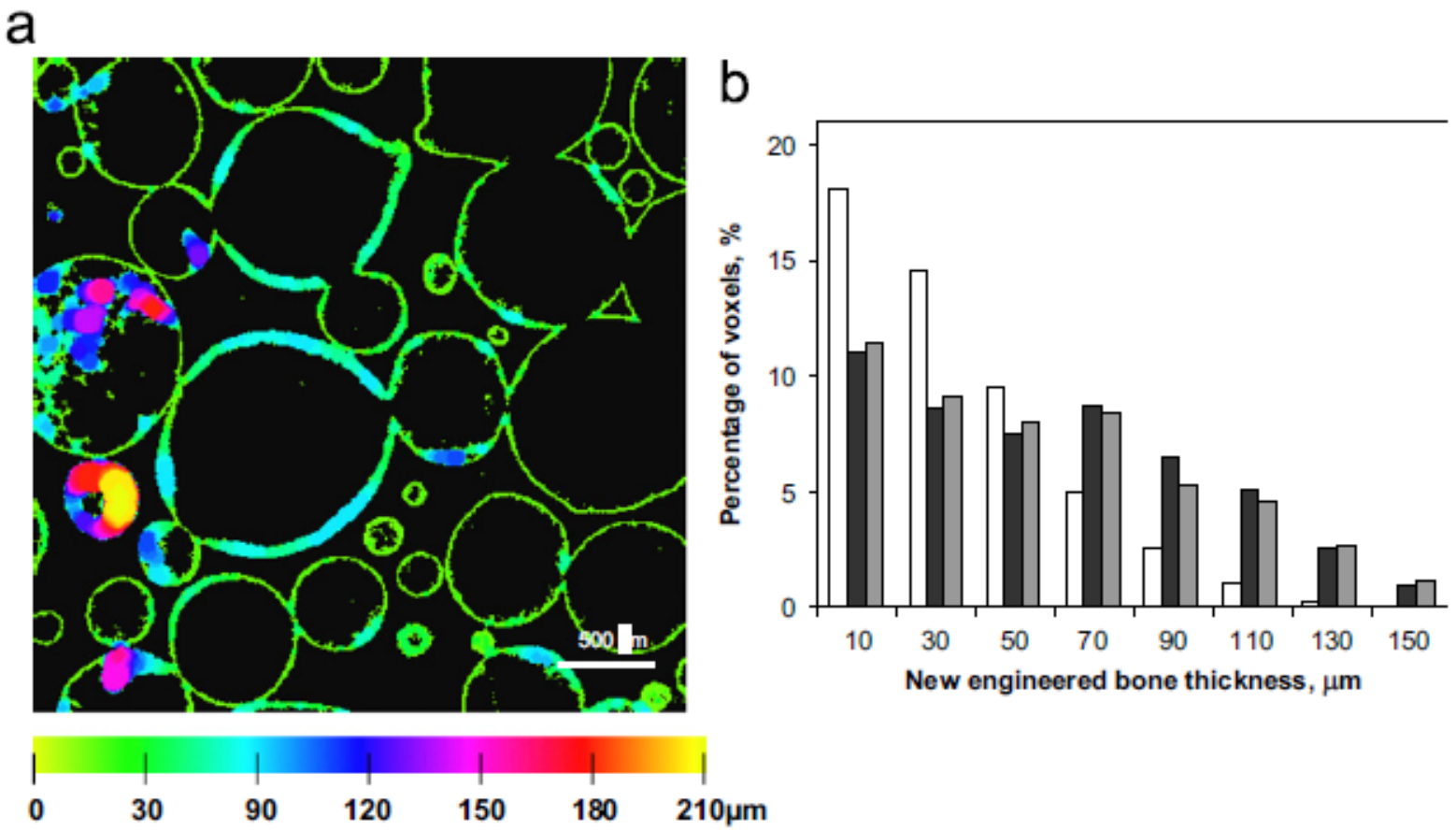

An example of a 2D slice within the 3D local new bone thickness at 8 weeks of implant (a). Histogram of the thickness distribution after 8 (empty columns), 16 (full columns), and 24 (striped columns) weeks of implant (b)

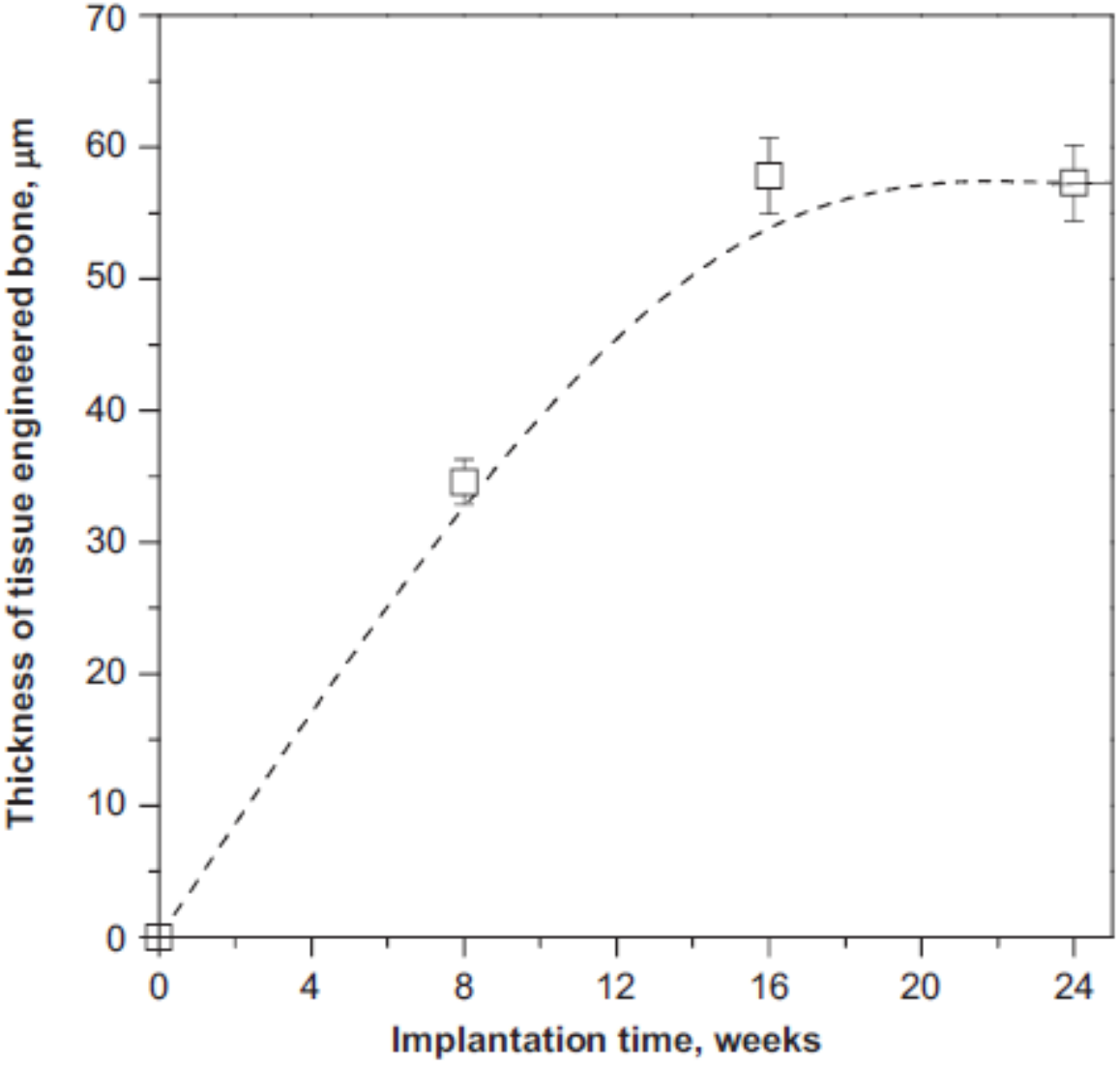
Thickness of tissue engineered bone, µm
70
60
50
40
30
20
10
0
0
4
8
12
16
20
24
Implantation time, weeks

Engineered bone from bone marrow stromal cells: a structural study by an advanced x-ray microdiffraction technique

CEDOLA, M. MASTROGIACOMO, M. BURGHAMMER, V. KOMLEV,
P. GIANNONI, R.CANCEDDA, F. RUSTICHELLI, A. FAVIA, S. LAGOMARSINO

Physics in Medicine and Biology, 51 (2006) p. 109-116

HA scaffold seeded with Bone Marrow Stromal Cells and implanted for 8 weeks in an immunodeficient mouse

Small Angle Scattering (SAXS) pattern

Digital zoom at small angles on WAXS pattern to obtain SAXS information in the same sample point

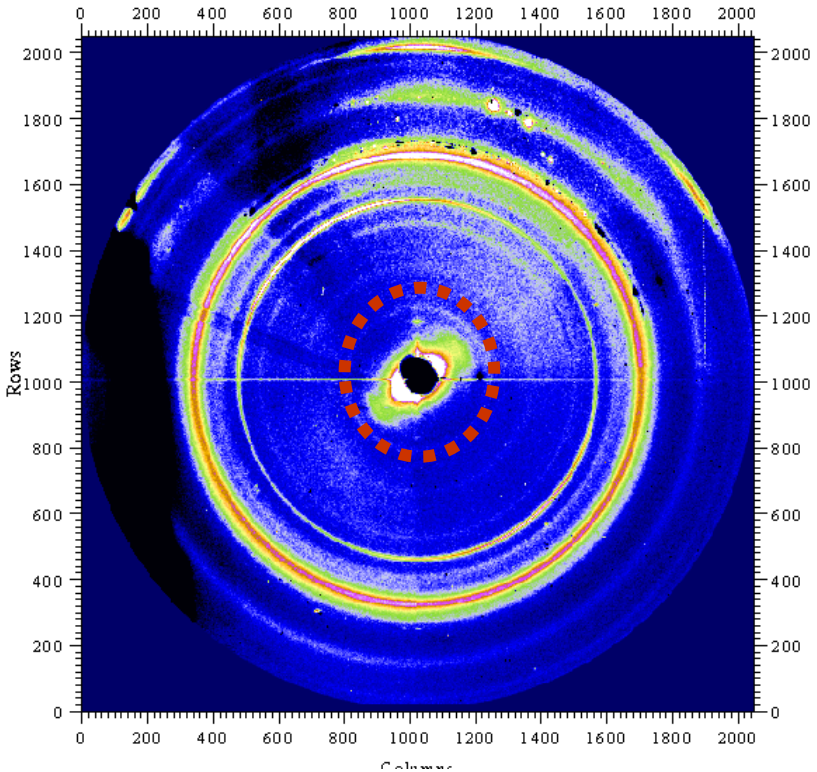

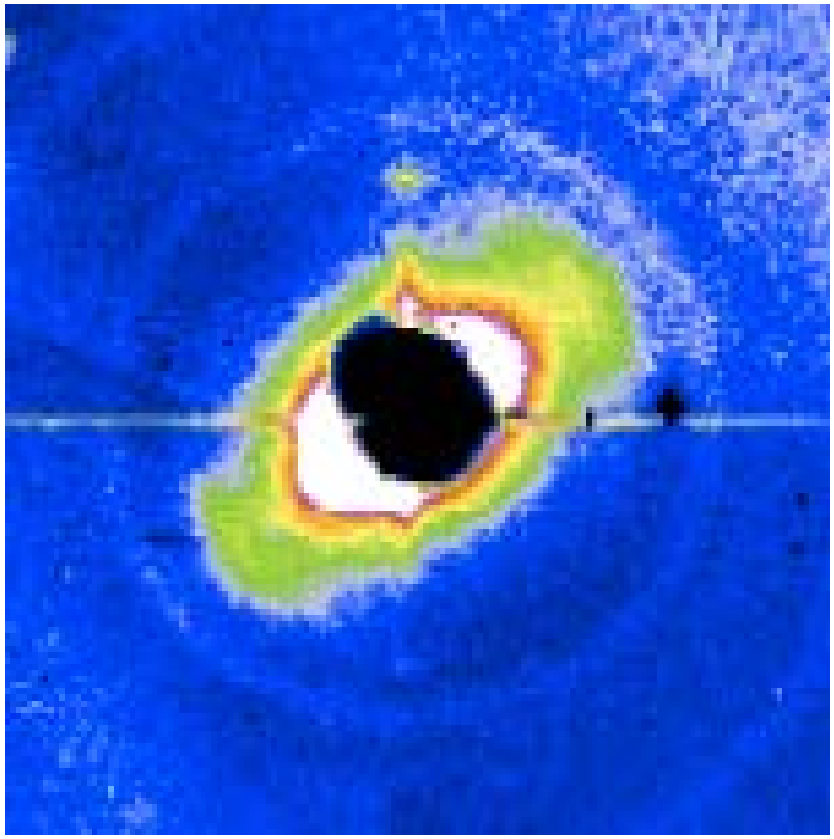

The central shadow is due to the beam-stopper while the white/brown/green intensity represents the SAXS image.

New bone – Orientation at porous surface

Collection of Small Angle Scattering (SAXS) patterns.
The evident anisotropy of SAXS patterns indicates that the mineral bone crystals are elongated and have a predominant orientation.

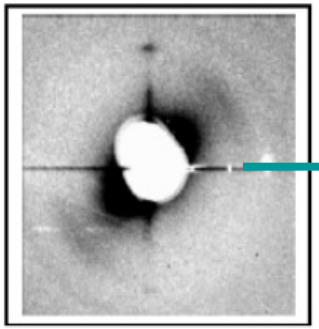

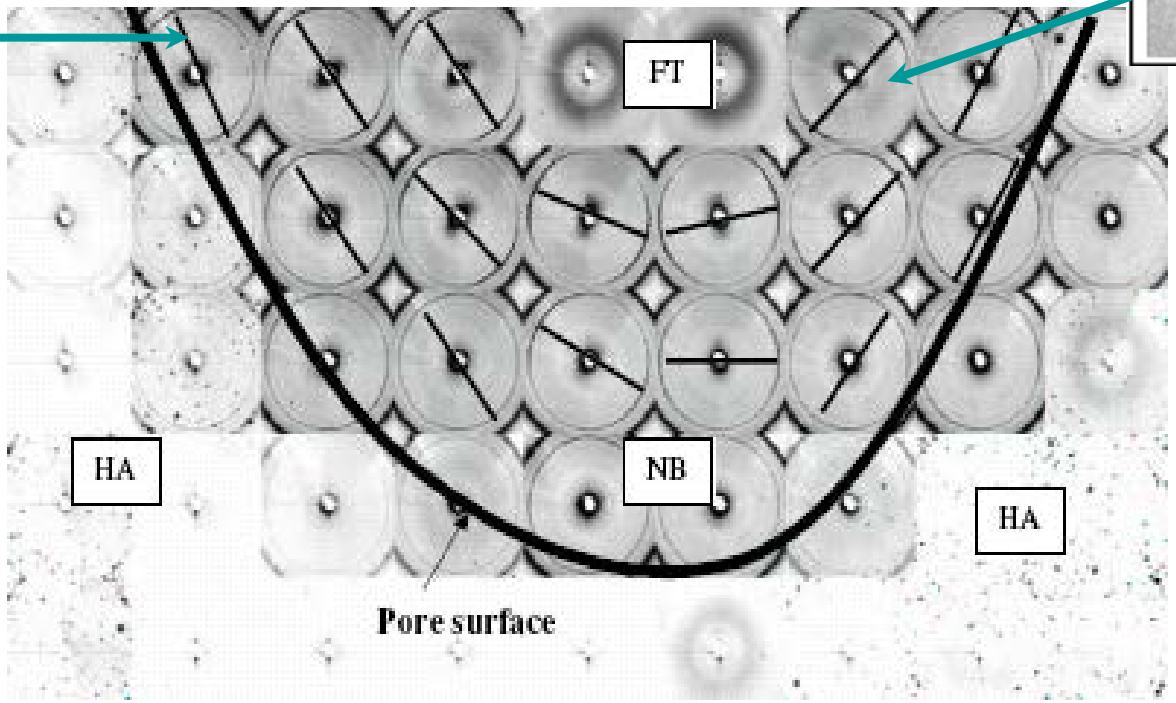

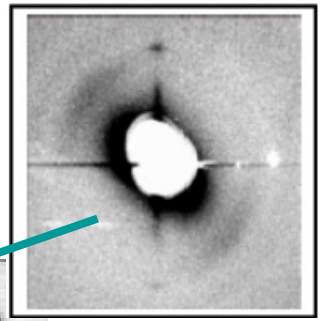

The collagen micro-fibrils

Blood Vessel 3d Visualization

X-Ray Synchrotron Radiation Pseudo-Holotomography as a New Imaging Technique to Investigate Angio- and Microvasculogenesis with No Usage of Contrast Agents

V. S. KOMLEV, M.MASTROGIACOMO, F. PEYRIN, R. CANCEDDA, F. RUSTICHELLI

Tissue Engineering, Part C, 15(2009), pag. 425-430

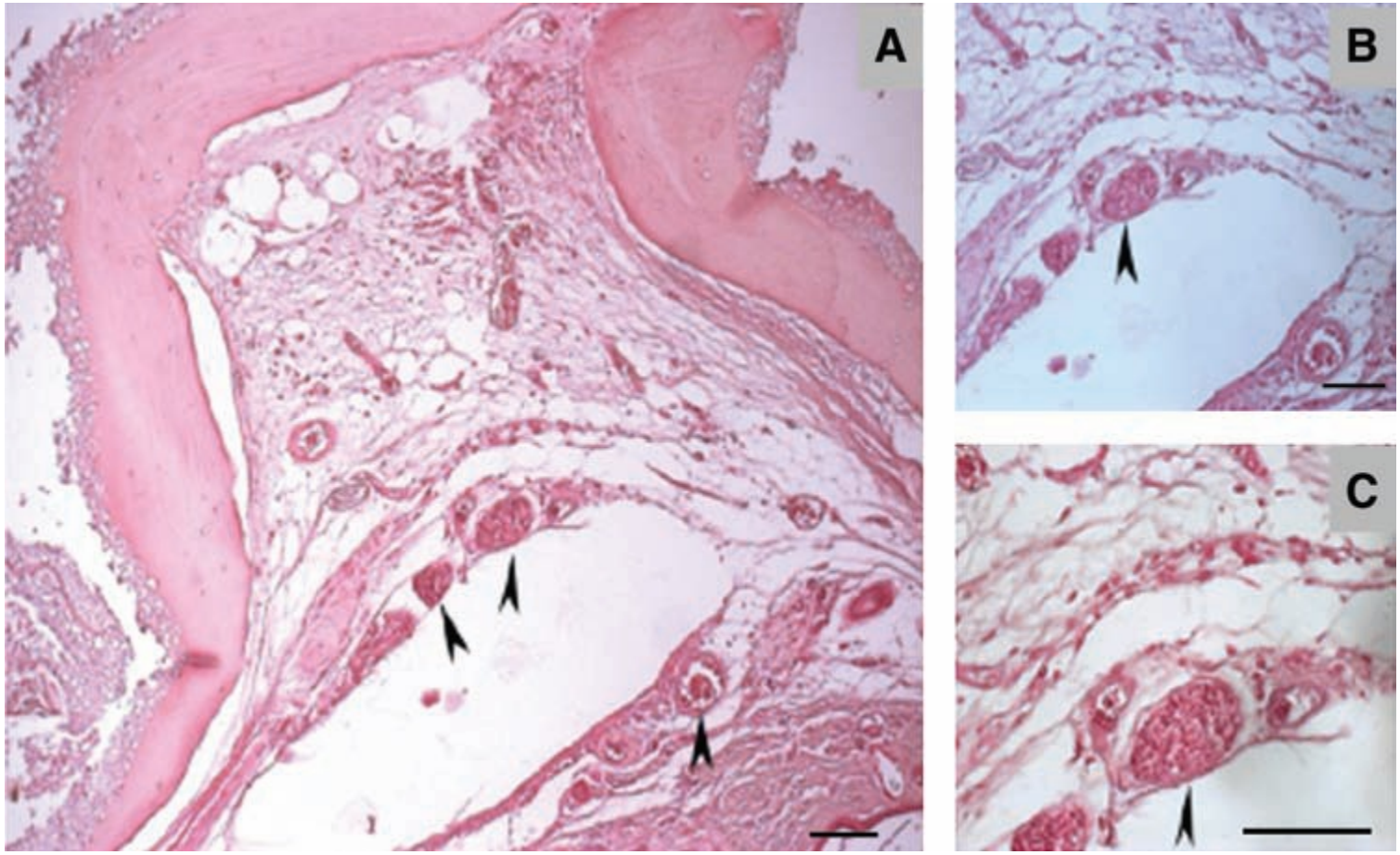

Histological images of a tissue-engineered construct (a SkeliteTM scaffold seeded with sheep MSC after 24 weeks of implantation in an immunocompromised mouse). Arrows indicate blood vessels. Panels (A) and (B) (scale bar is 100mm) are enlargements of panel (C) (scale bar is 50 mm)

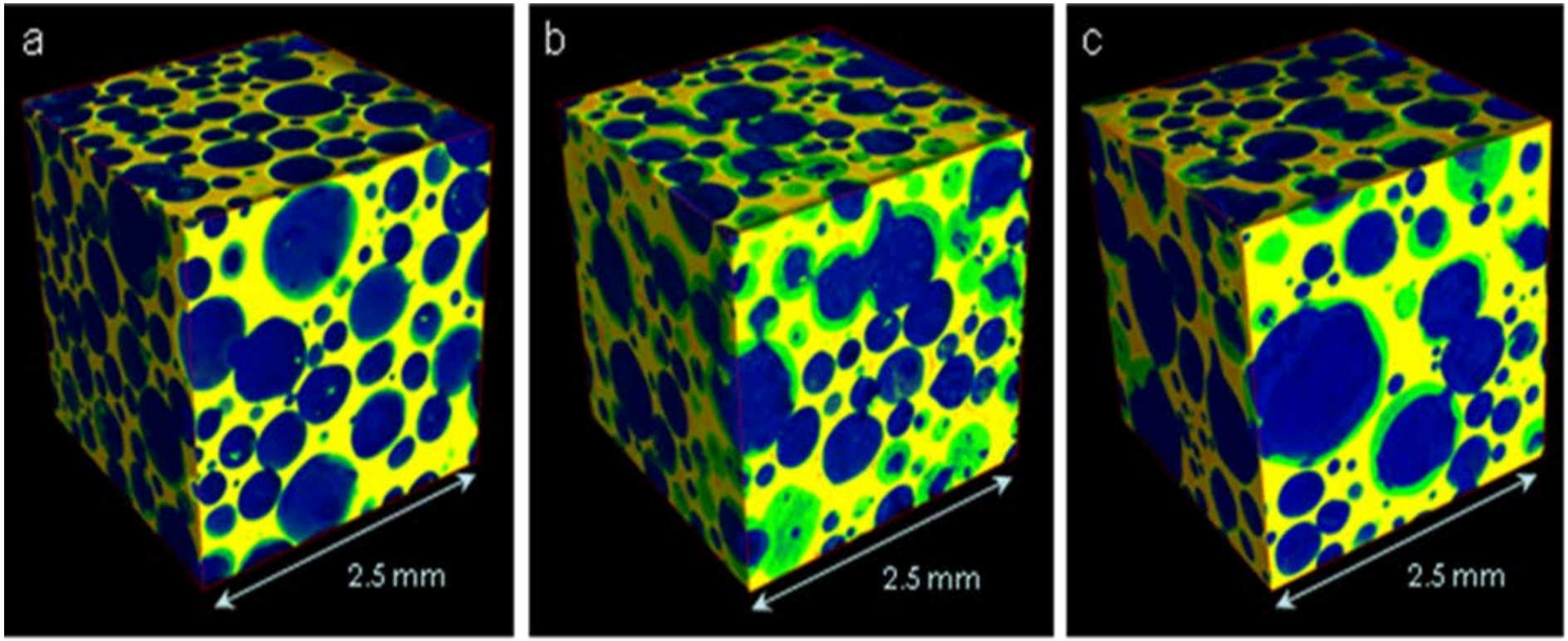

3D Micro-CT image of the tissue-engineered construct after 24 weeks of implantation in an immunocompromised mouse.

Holo-tomography at the ID19 Beamline (ESRF, F)

1. Phase Retrieval with images at four different distances in order to get a phase map.

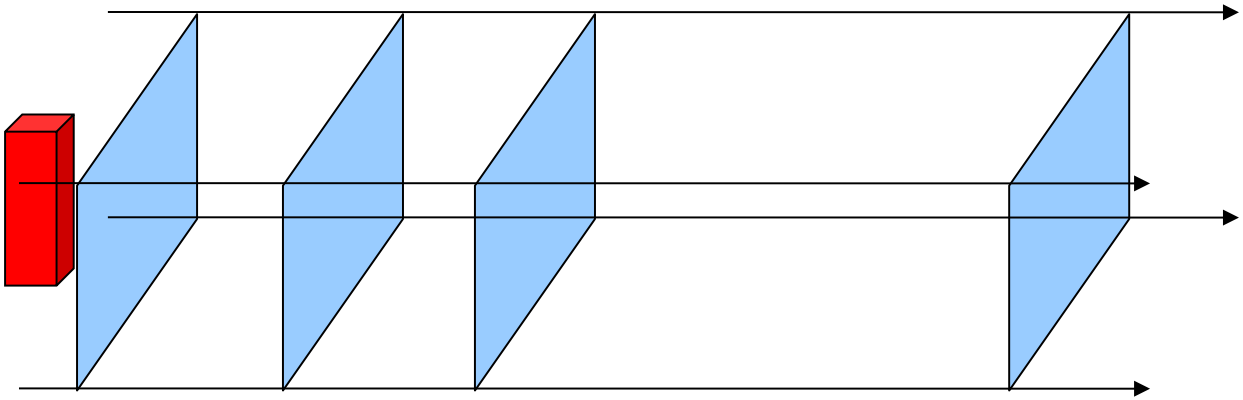

D1= 7 mm D2= 29 mm D3= 59 mm D4= 119 mm

2. Tomography: Repeated for 1500 angular Projections;

3. Experimental Conditions:
Energy: 20 keV;
Pixel size: 700 nm.

3D Pseudo- holotomographic images of the tissue-engineered construct after 24 weeks of implantation in an immunocompromised mouse. The images show the vessels' ingrowth inside the scaffold: vessels' growth occurred both in the presence (A, green) and in the absence of newly formed bone (B, brown=pink). Details of 3D spatial distribution of the phases into scaffolds within one single pore (C, D).

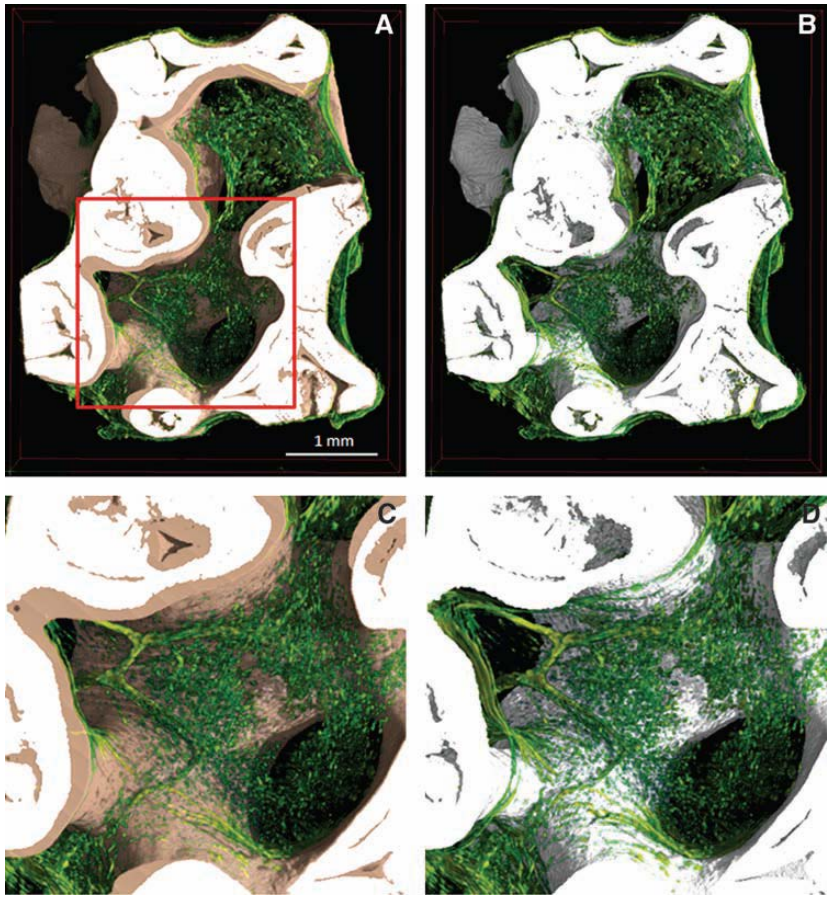

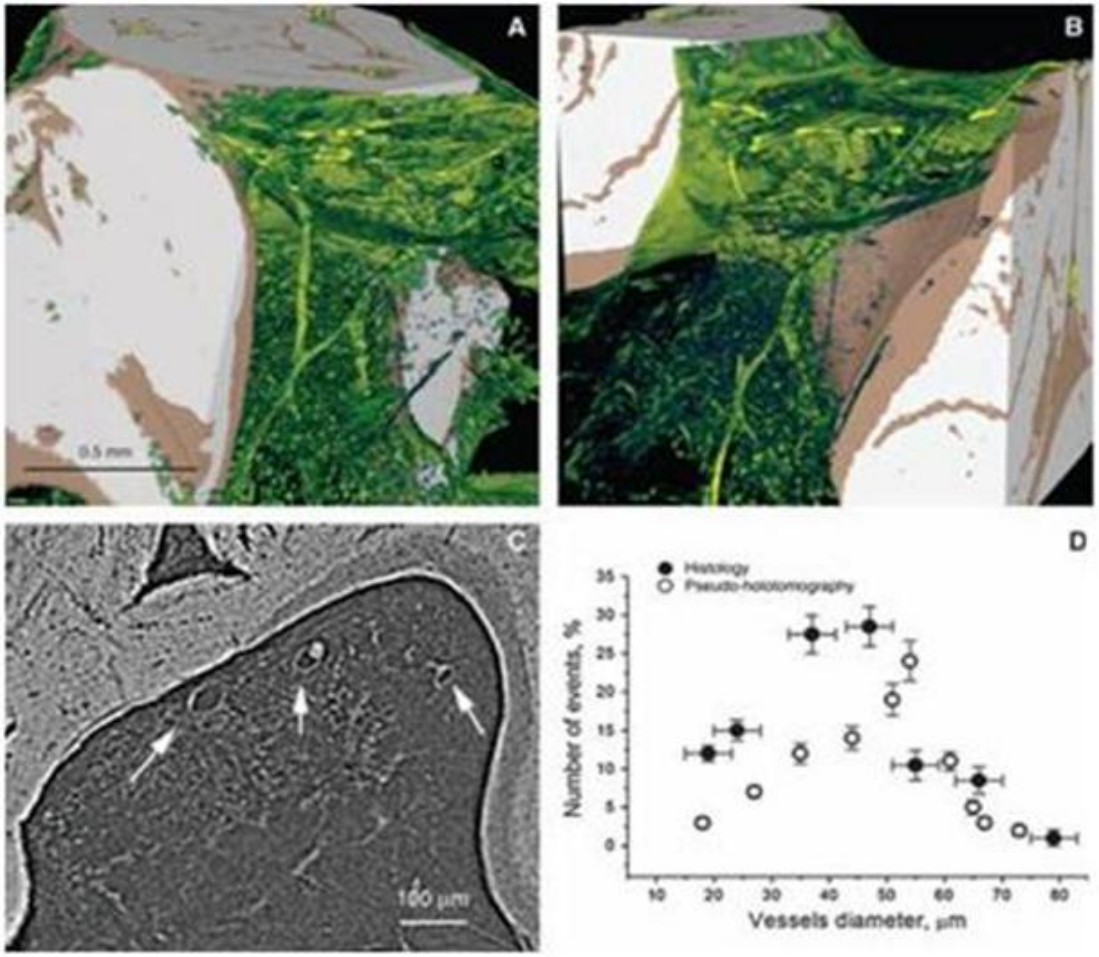

Statistical information of the 3D vessel network imaging (A, B) and 2D micro-CT image (C). (D) Histogram of the vessel diameter distribution measured for pseudo-holotomography data (open circle) and histology (solid circle)

TISSUE ENGINEERING: Part C
Volume 15, Number 00, 2009

DOI: 10.1089/ten.tec.2008.0270

Organization of Extracellular Matrix Fibers Within Polyglycolic Acid–Polylactic Acid Scaffolds Analyzed Using X-Ray Synchrotron-Radiation Phase-Contrast Micro Computed Tomography

Gianni Albertini, M.D.,[1,2] Alessandra Giuliani, Ph.D.,[2,3,4] Vladimir Komlev, Ph.D.,[3] Francesca Moroncini, Ph.D.,[1,2] Armanda Pugnaloni, Ph.D.,[5] Giuseppina Pennesi, M.D., Ph.D.,[6] Marzia Belicchi, Dott.,[7] Corrado Rubini,[8] Franco Rustichelli, Ph.D.,[2,3,4] Roberta Tasso, Ph.D.,[9] and Yvan Torrente, Ph.D.[7]

Spatio temporal organized patterns of cell surface–associated and extracellular matrix (ECM)-embedded molecules play important roles in the development and functioning of tissues. ECM proteins interact with the surface of bioscaffold polymers and influence material-driven control of cell differentiation.

Using X-ray phase-contrast micro computed tomography (microCT), we visualized the three-dimensional (3D) image of ECM organization after in vitro seeding of bone marrow–derived human and murine mesenchymal stem cells (MSCs) induced to myogenic differentiation, labelled with iron oxide nanoparticles, and seeded onto polyglycolic acid–polylactic acid scaffolds.

Polymer scaffolds + stem cells

PGA/PLLA scaffolds cultured without cells

PGA/PLLA scaffolds cultured with Human mesenchymal stem cells

PGA/PLLA scaffolds cultured with Murine mesenchymal stem cells

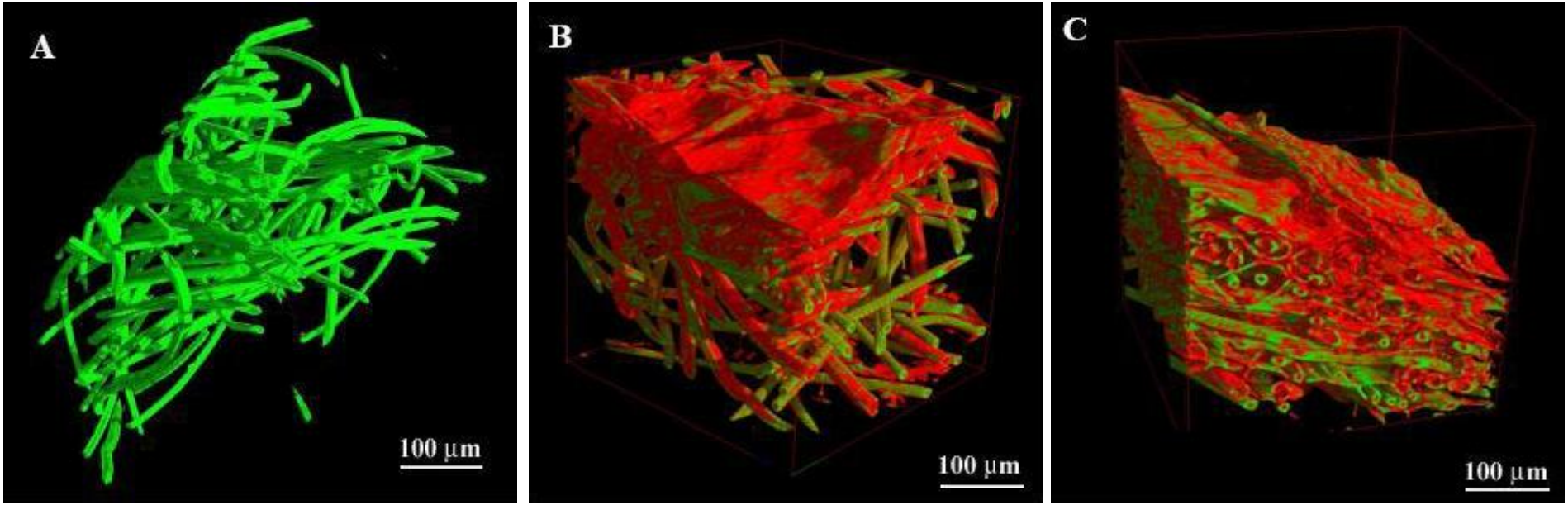

Fiber scaffold (green), thin Extracellular Matrix ECM (red).

3D display of the scaffold and fiber phase cultured with murine-MSC

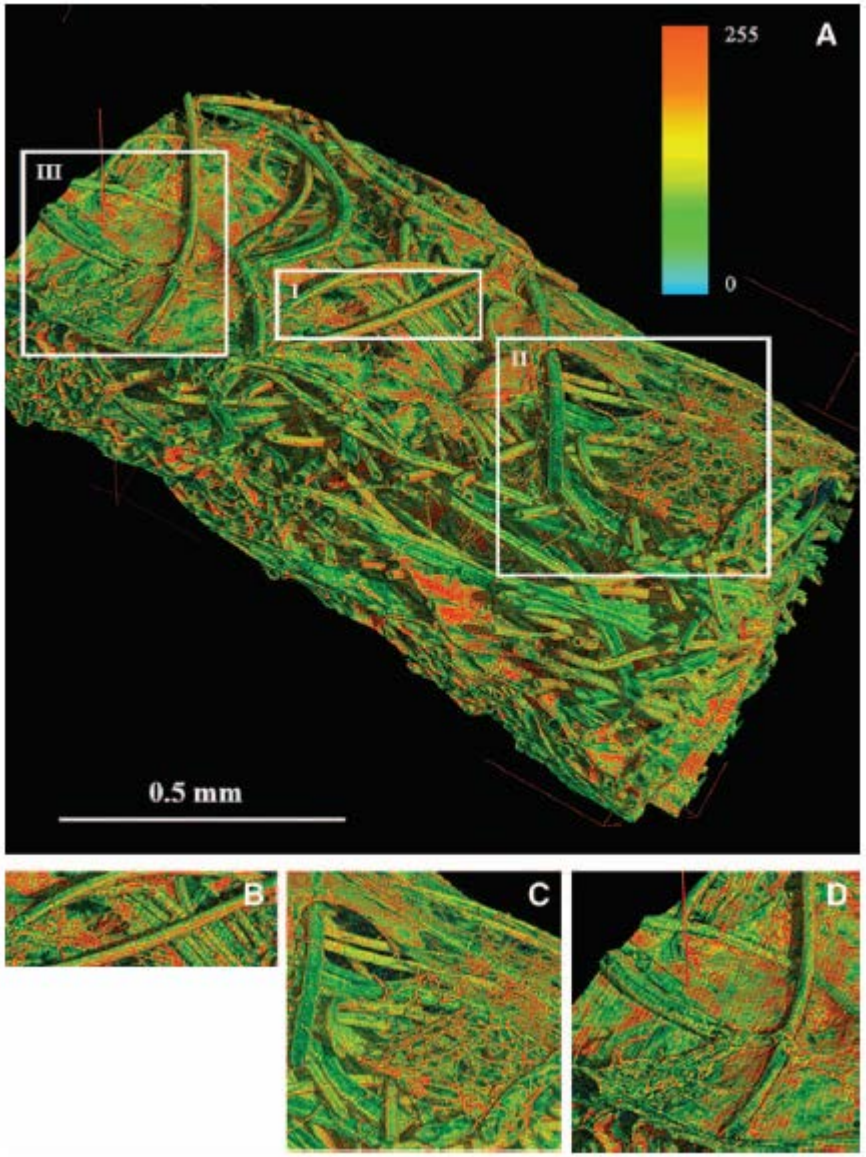

Extracellular matrix detection using X-ray micro computed tomography. Three-dimensional display of the scaffold fibers and of the deposited matrix (A).

The ‘‘stages’’ were zoomed in. The matrix fibrils were initially deposited on the scaffold fibers (Stage I) (B).
At Stage II, they appear to be organized in chains at different sites (C).
At Stage III, chains appear to be organized as networks at different sites, indicating that the aggregation process contributes to developing matrix layers (D).

Novel insight into stem cell trafficking in dystrophic muscles

A.Farini, C.Villa, A.Manescu, F.Fiori, A.Giuliani, P.Razini, C.Sitzia, G.Del Fraro, M.Belicchi, M.Meregalli, F.Rustichelli, Y.Torrente,

International Journal of Nanomedicine

7 (2012) 3059-3067.

Ivan Torrente and coworker were able to regenerate muscular tissue in dystrophic muscles by injecting human stem cells

[M.Sampaolesi et al., Science 301 (2003) 487]

•The homing in the muscular tissue of these stem cells, at different times after injection in dystrophic mice, was investigated *in-vivo* by micro-CT at ESRF, after labeling them by Fe_3O_4 (Endorem) nanoparticles

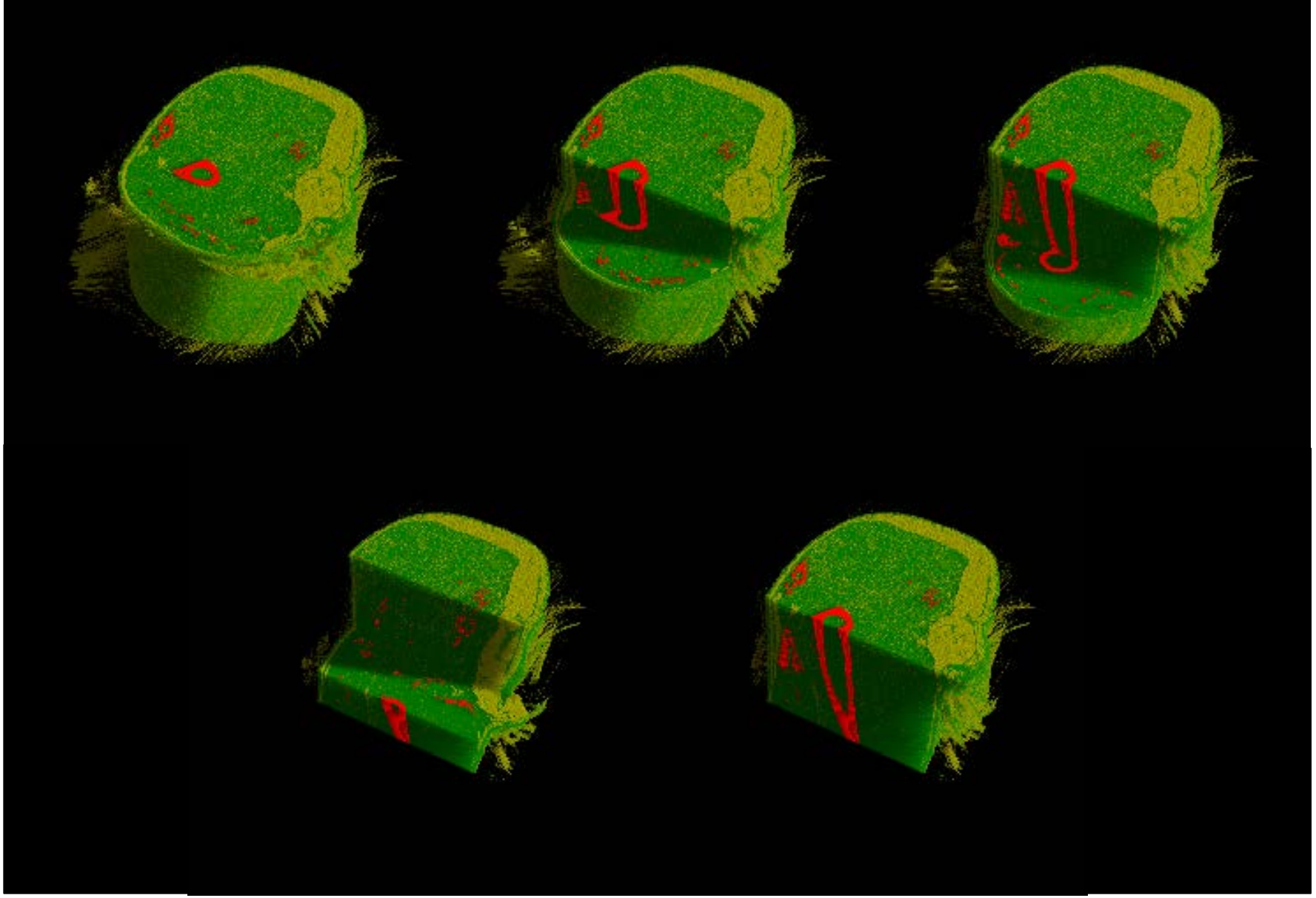

15 Minutes After injection intro-arteria

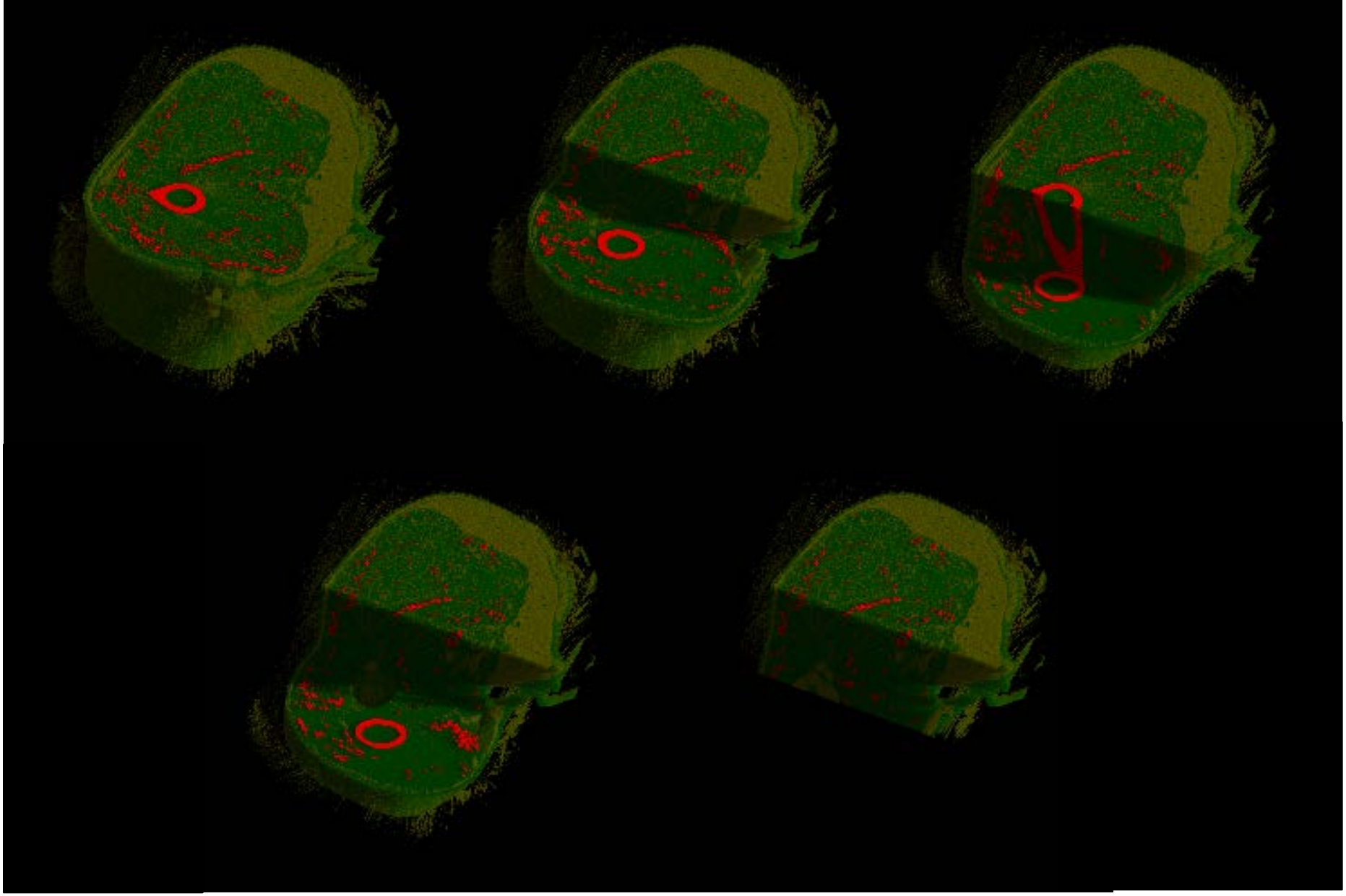

2 Hours After injection intro-arteria

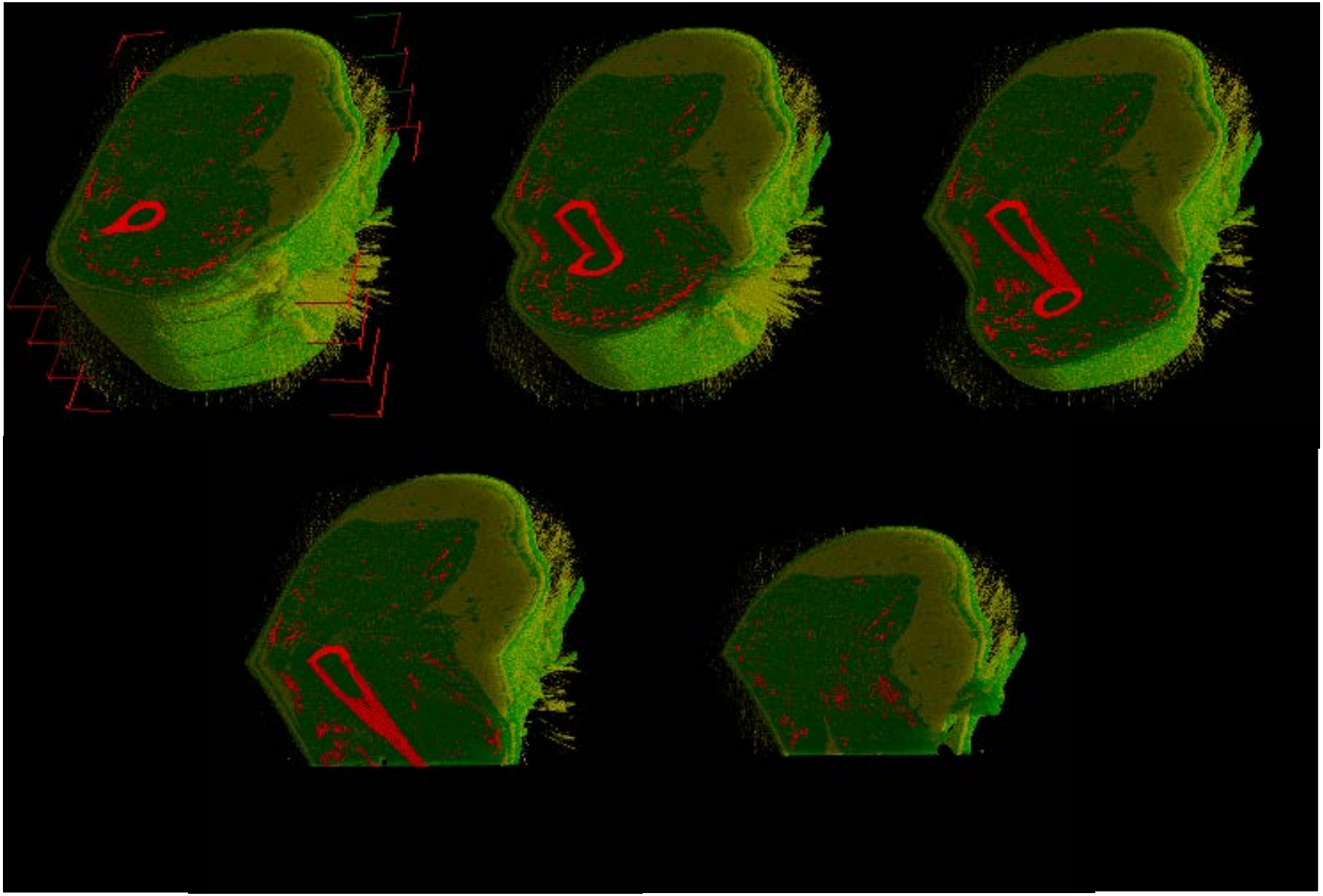

13 Hours After injection intro-arteria

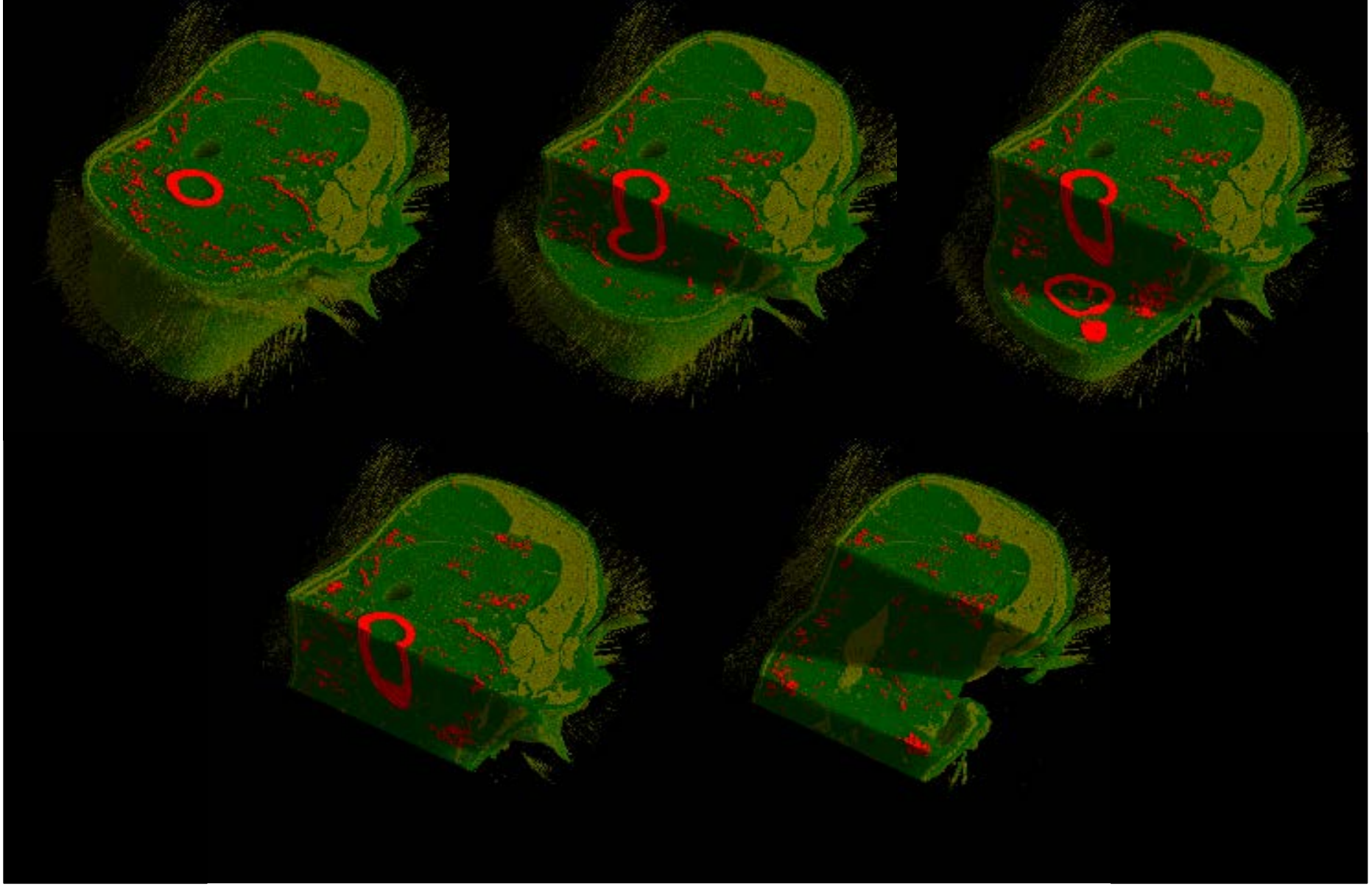

24 Hours After injection intro-arteria

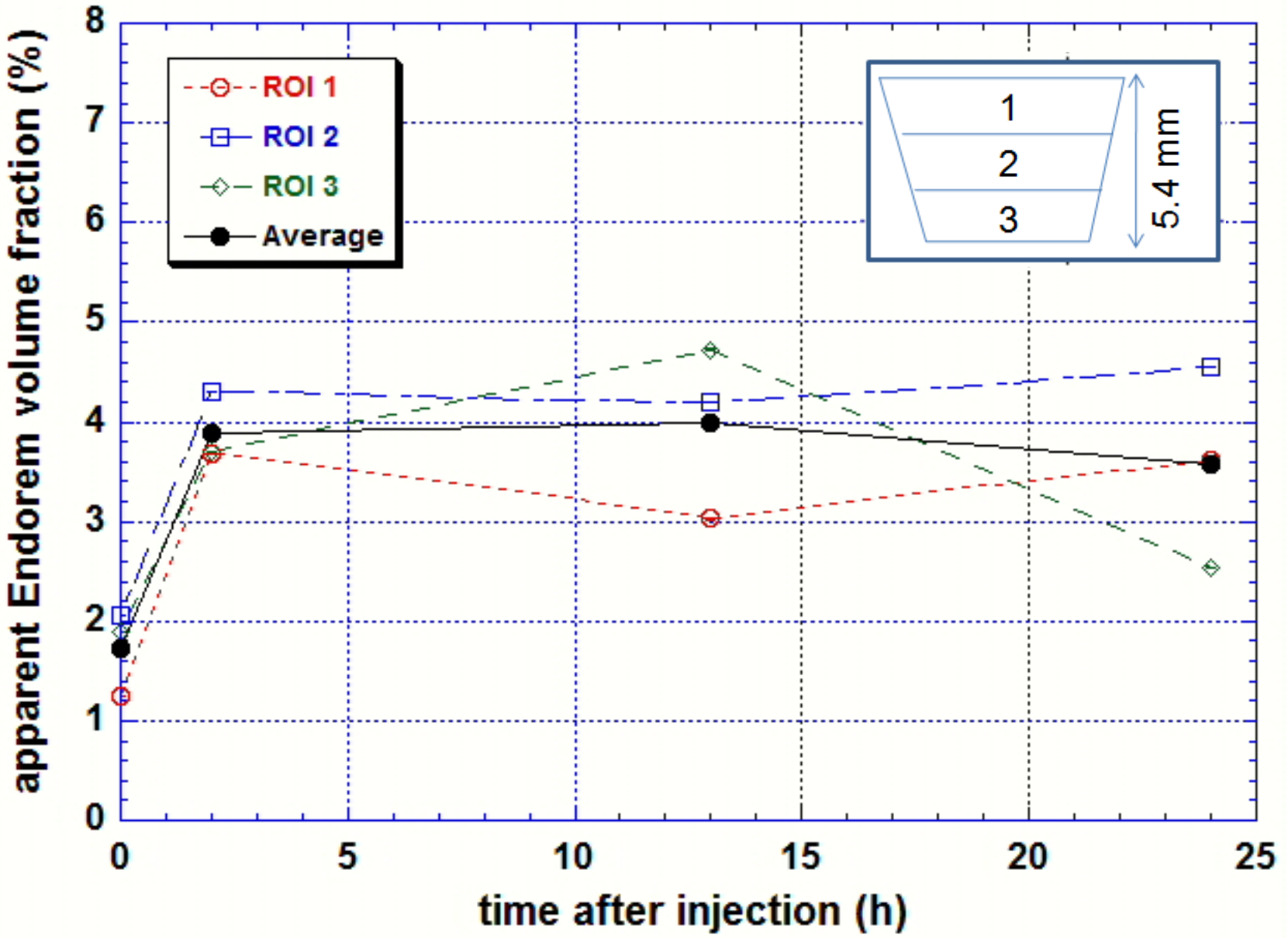
ROI 1
ROI 2
ROI 3
Average
1
2
3
5.4 mm
apparent Endorem volume fraction (%)
time after injection (h)
0
1
2
3
4
5
6
7
8
0
5
10
15
20
25

Conclusion

We demonstrated that migration of intra-arterially delivered stem cells to dystrophic muscles is time dependent, and that the number of migrating cells increases specifically in damaged muscle tissues. Moreover, our findings suggest that a better understanding of the kinetic of distribution and migration of the stem cells is crucial for enhancing the therapeutic potential of these cells in tissue repair.